(12) INTERNATIONAL APPLICATION PUBLISHED UNDER THE PATENT COOPERATION TREATY (PCT)

(19) World Intellectual Property Organization
International Bureau

(43) International Publication Date
19 July 2007 (19.07.2007)

PCT

(10) International Publication Number
WO 2007/081705 A2

(51) International Patent Classification:
G06F 17/50 (2006.01)

(21) International Application Number:
PCT/US2007/000071

(22) International Filing Date: 4 January 2007 (04.01.2007)

(25) Filing Language: English

(26) Publication Language: English

(30) Priority Data:
60/756,038 4 January 2006 (04.01.2006) US

(71) Applicant *(for all designated States except US)*: **UNIVERSITY OF SOUTH FLORIDA** [US/US]; 3802 Spectrum Boulevard, Suite 100, Tampa, FL 33612 (US).

(72) Inventors; and

(75) Inventors/Applicants *(for US only)*: **LIU, Jiang** [CN/US]; 417 Greenbriar Drive, #6, Normal, IL 61761 (US). **DUNLEAVY, Lawrence, P.** [US/US]; 4202 East Fowler Avenue, ENB 118, Tampa, FL 33620 (US). **VESPECHT, Jan** [BE/BE]; Gertrudevelt 15, B-1840 Steenhuffel (BE).

(74) Agent: **MCGAW, Michael, M.**; Smith & Hopen, P.A., 180 Pine Avenue North, Oldsmar, FL (US).

(81) Designated States *(unless otherwise indicated, for every kind of national protection available)*: AE, AG, AL, AM, AT, AU, AZ, BA, BB, BG, BR, BW, BY, BZ, CA, CH, CN, CO, CR, CU, CZ, DE, DK, DM, DZ, EC, EE, EG, ES, FI, GB, GD, GE, GH, GM, GT, HN, HR, HU, ID, IL, IN, IS, JP, KE, KG, KM, KN, KP, KR, KZ, LA, LC, LK, LR, LS, LT, LU, LV, LY, MA, MD, MG, MK, MN, MW, MX, MY, MZ, NA, NG, NI, NO, NZ, OM, PG, PH, PL, PT, RO, RS, RU, SC, SD, SE, SG, SK, SL, SM, SV, SY, TJ, TM, TN, TR, TT, TZ, UA, UG, US, UZ, VC, VN, ZA, ZM, ZW.

(84) Designated States *(unless otherwise indicated, for every kind of regional protection available)*: ARIPO (BW, GH, GM, KE, LS, MW, MZ, NA, SD, SL, SZ, TZ, UG, ZM, ZW), Eurasian (AM, AZ, BY, KG, KZ, MD, RU, TJ, TM), European (AT, BE, BG, CH, CY, CZ, DE, DK, EE, ES, FI, FR, GB, GR, HU, IE, IS, IT, LT, LU, LV, MC, NL, PL, PT, RO, SE, SI, SK, TR), OAPI (BF, BJ, CF, CG, CI, CM, GA, GN, GQ, GW, ML, MR, NE, SN, TD, TG).

Published:

— *without international search report and to be republished upon receipt of that report*

[Continued on next page]

(54) **Title:** METHOD OF CHARACTERIZING NONLINEAR BEHAVIOR OF AMPLIFIERS USING LOADPULL MEASUREMENTS

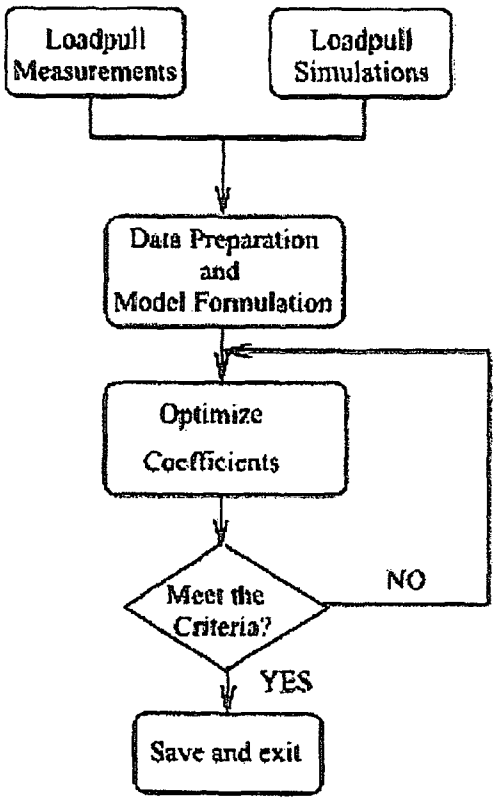

(57) **Abstract:** A behavioral modeling technique is provided that is based directly on the loadpull gain and phase compression measurements. Developed from the large-signal scattering function theory, this technique shows the possibility to generate the large- signal scattering function model using traditional toadpull measurement systems. The large-signal scattering function theory is presented and the analogy between the LSNA and the loadpull measurement systems is drawn. A detailed analysis of the model generation process is further taught herein.

WO 2007/081705 A2

For two-letter codes and other abbreviations, refer to the "Guidance Notes on Codes and Abbreviations" appearing at the beginning of each regular issue of the PCT Gazette.

METHOD OF CHARACTERIZING NONLINEAR BEHAVIOR OF AMPLIFIERS USING LOADPULL MEASUREMENTS

CROSS REFERENCE TO RELATED APPLICATIONS

This application claims priority to currently pending U.S. Provisional Patent Application 60/756,038, entitled, "Behavior Model for Nonlinear Ampifiers/Devices Using Loadpull Measurements", filed January 04, 2006, the contents of which are herein incorporated by reference.

FIELD OF INVENTION

This invention relates to radio frequency and microwave technology. More specifically, this invention relates to the characterization of the nonlinear behavior of amplifiers and other devices using loadpull measurement.

BACKGROUND OF THE INVENTION

Radio frequency (RF) and microwave devices exhibit linear signal behavior that is generally characterized by S-parameters. Traditionally, the S-parameter approach was satisfactory for characterizing the signal behavior of most RF and microwave devices and applications. However, with the advance of modern wireless communication systems, more and more demands are generated for nonlinear operation of devices and amplifiers to get better transmission efficiency and less power consumption. This causes distortion effects, such as harmonics and spectral regrowth. The classical S-parameter theory is no longer suitable for this situation.

SUMMARY OF INVENTION

A behavioral modeling technique is provided that is based directly on the loadpull gain and phase compression measurements. Developed from the large-signal scattering function theory, this technique shows the possibility to generate the large-

signal scattering function model using traditional loadpull measurement systems. The large-signal scattering function theory is presented and the analogy between the LSNA and the loadpull measurement systems is drawn. A detailed analysis of the model generation process is further taught herein.

BRIEF DESCRIPTION OF THE DRAWINGS

For a fuller understanding of the invention, reference should be made to the following detailed description, taken in connection with the accompanying drawings, in which:

FIG. 1 is a diagram illustrating a two port network with the voltage and current definition.

FIG. 2 illustrates the input and output variables for a two-port network used in the large- signal scattering function are composed of the fundamental tones as well as the harmonics for both the incident and reflected waves.

FIG. 3 is a diagram illustrating the functional block of the LSNA.

FIG. 4 illustrates the interpolation and extrapolation problem due to the insufficient testing points with the file-based model.

FIG. 5 is a diagram of a two-port network with a voltage source of E_s and source impedance of Z_s. The load impedance is Z_L.

FIG. 6 is a flowchart of the Matlab program created for the behavioral model optimization based on the loadpull AM-AM and AM-PM datasets.

FIG. 7 is an illustration of the MAXIM 2373 LNA sample.

FIG. 8 is a graph illustrating a comparison of the measured and simulated gain and phase compression at 50 ohm.

FIG. 9 illustrates the simulated output power contours compared with the measurements. The input power is at -30dBm.

FIG. 10 illustrates a comparison of simulated and measured output power contours. The new model and the large-S21 model are compared side by side, showing the improvement of the new model to predict the changing optimal load impedance.

FIG. 11 illustrates a comparison of the measured and simulated IP3 using the large-signal behavioral model.

FIG. 12 is an illustration of the six load impedance examples on the Smith Chart. The six loads spread in a large area, showing the robustness of this model to predict the nonlinear effect in a wide load range.

FIG. 13 is a set of graphs illustrating a comparison of the measured and simulated Pout and IM3 at 6 load impedances.

FIG. 14 is a graph illustrating the errors of the simulated fundamental tone at 6 loads. The brackets on the right illustrate the plots associated with the newly developed model and the large-S21 model as indicated. The new model presents better performance, compared with the large-S21 model.

FIG. 15 is a graph illustrating the errors of the simulated 3rd order intermodulation product at 6 loads. The brackets on the right illustrate the plots associated with the newly developed model and the large-S21 model as indicated. The new model presents better performance, compared with the large-S21 model.

FIG. 16 is an illustration of the ISL3984 power amplifier sample.

FIG. 17 is a pair of graphs illustrating a comparison of the simulated and measured gain and phase compression in 50 ohm.

FIG. 18 is an illustration showing a comparison of the simulated output power contour with the measured dataset.

FIG. 19 is an illustration showing a comparison of the simulated IM3 contour using the behavioral model with the measured dataset.

FIG. 20 is an illustration of the six load impedance examples used to test the behavioral model developed for the ISL3984 on the Smith Chart. The six loads spread in a large area, showing the robustness of this model to predict the nonlinear effect in a wide load range.

FIG. 21 is a set of graphs showing a comparison of the measured and simulated Pout and IM3 at 6 load impedances.

FIG. 22 is a graph illustrating the errors of the simulated fundamental tone at 6 loads. The brackets on the right illustrate the plots associated with the newly developed model and the large-S21 model as indicated. The new model presents better performance, compared with the large-S21 model.

FIG. 23 is a graph illustrating the errors of the simulated 3rd order intermodulation product at 6 loads are plotted. The brackets on the right illustrate the plots associated with the newly developed model and the large-S21 model as indicated. The new model presents better performance, compared with the large-S21 model.

FIG. 24 is a pair of graphs illustrating a comparison of the simulated gain and phase compression under 50 ohm condition: behavioral model vs. circuit model.

FIG. 25 is an illustration showing a comparison of the simulated Pout contours from the behavioral model and the circuit model at constant Pin of 10 dBm.

FIG. 26 is an illustration showing a comparison of the simulated Pout contours from the behavioral model and the circuit model at constant Pin of 30 dBm.

FIG. 27 is an illustration showing a comparison of the simulated IM3 contours from behavioral models: one optimized with loadpull AM-PM information and one without.

FIG. 28 is an illustration showing a comparison of the simulated IM3 contours from the behavioral and circuit models.

FIG. 29 is a pair of graphs illustrating a comparison of the simulated IM3 from the circuit model and the behavioral models. Behavioral model 1 is created with the loadpull AM-PM information, while behavioral model 2 isn't. The simulated IM3 Behavioral model 2 shows a fake sweet spot, showing the importance to have the loadpull AM-PM information in the model generation process. The Γ_L is at -0.80213 - j * 0.08629.

DETAILED DESCRIPTION OF THE PREFERRED EMBODIMENT

Large-signal scattering function theory is proposed to address limitations in the S-parameter approach. In general, this theory extends the small-signal theory to take into account not only the fundamental, but also harmonics at different ports. The

contribution of all these spectral components is formulated into nonlinear functions, therefore, making it possible to characterize the nonlinearities. A specific measurement system, called a large-signal network analyzer (LSNA), is required to measure and derive this type of large-signal behavioral model. This theory hasn't been widely applied due to the limited access to such specialized (and costly) systems.

By closely studying the large-signal scattering function theory, useful large-signal models can be derived from the loadpull measurement system, although some advanced measurement procedures are required. We present the procedure for deriving the behavioral model and example modeling results are demonstrated showing proof of principle.

The disclosed modeling technique also provides a solution to fully utilize the loadpull measurement dataset. Although the loadpull measurement has been widely applied in power devices (or amplifiers) characterization and design, derivation of an accurate behavioral model from the dataset still presents as a huge challenge. Most of the time, the loadpull measurement datasets are only used for observation of the optimal load points or as a verification for the device modeling. There are some commercially available solutions in current microwave circuit simulation software, such as the Advanced Design System (ADS) and the Microwave Office, to generate behavioral models from the measurement datasets, however, the model has limitations. The method disclosed shows an analytical way to exploit the datasets and presents significant advantages over the existing approaches.

The theory of the large-signal scattering function is first introduced. The limitations of the current modeling techniques then elaborated. The detailed derivation and optimization process of the instant method is then presented. Three example models are constructed and detailed in the examples that follow. Their simulation results are then compared with measurement results. Good agreements observed prove the effectiveness of the proposed modeling technique.

Small signal network analysis

An N-port linear network can be fully characterized by capturing the relationship between the current and voltage at each port. A two port network as shown in FIG. 1, can be fully described through Z, Y, ABCD or S-parameters.

For example, the Y parameter for this two-port network is given in Equation 1:

$$\begin{bmatrix} i_1 \\ i_2 \end{bmatrix} = \begin{bmatrix} y_{11} & y_{12} \\ y_{21} & y_{22} \end{bmatrix} \begin{bmatrix} v_1 \\ v_2 \end{bmatrix} \quad (1)$$

where i_n and v_n, are the current and voltage at port n, y_{mn} is the admittance from port n to port m with port m shorted. The Y-parameter can be determined using short circuited outputs, i.e. the y, can be determined through Equation 2 by shorting the port i:

$$y_{mn} = \left.\frac{i_m}{v_n}\right|_{v_m=0} \quad (2)$$

Similarly, Z parameter is defined in Equation 3. To obtain the Z-parameter, open circuited outputs are required, as indicated in Equation 4.

$$\begin{bmatrix} v_1 \\ v_2 \end{bmatrix} = \begin{bmatrix} z_{11} & z_{12} \\ z_{21} & z_{22} \end{bmatrix} \begin{bmatrix} i_1 \\ i_2 \end{bmatrix} \quad (3)$$

$$z_{mn} = \left.\frac{v_m}{i_n}\right|_{i_m=0} \quad (4)$$

However, when dealing with high frequencies, these parameter definitions are no longer suitable. First, the ideal short and open circuit are difficult to obtain at high frequencies. Second, the voltage and the current are difficult to measure at high frequencies. Therefore, the scattering parameter is proposed to solve these problems. The idea is to measure the incident, reflected and transmitted waveforms to capture the performance of the network studied. The ingoing wave a and outgoing wave b are defined as:

$$a = \frac{v + Z_0 \cdot i}{\sqrt{2\mathrm{Re}(Z_0)}} \qquad b = \frac{v - Z_0^* \cdot i}{\sqrt{2\mathrm{Re}(Z_0)}} \quad (5)$$

where Z_0 is the reference impedance.

The S-parameter is defined in Equation 6, as a function of frequency *f*:

$$\begin{bmatrix} b_1(f) \\ b_2(f) \end{bmatrix} = \begin{bmatrix} s_{11}(f) & s_{12}(f) \\ s_{21}(f) & s_{22}(f) \end{bmatrix} \begin{bmatrix} a_1(f) \\ a_2(f) \end{bmatrix} \quad (6)$$

The S-parameter can be determined by terminating all other ports instead of port j with matched loads to avoid reflection and interference.

$$s_{ij}(f) = \left. \frac{b_i(f)}{a_j(f)} \right|_{a_i(f)=0} \quad (7)$$

The Z, Y or S-parameters can be considered as behavioral models, since they deal with only the port variables and don't require information about the internal structure of the network. All the network parameter sets have one important assumption, that is the network is linear and superposition is valid. When the network shows nonlinear effects, typically through the generation of new frequencies (harmonics or mixing products), the Z, Y or S-parameters are no longer valid and more advanced methods are required to characterize the network.

Theory of the large-signal scattering function

The large signal scattering function has been proposed to extend the applicability of the small-signal (linear) S-parameter concept. The idea of the large-signal S-parameter was in existence since 1997. Recently, a new broadband version of the original theory was presented in Verspecht et al. (2005), which extends this modeling technique to add the frequency dimension (J. Verspecht, D. Root, J. Wood, and A. Cognata, "Broad-band, multi-harmonic frequency domain behavioral models from automated large-signal vectorial network measurements," in *IEEE MTT-S Digest,* June 2005.).

As introduced in Verspecht et al. (1997) and Verspecht et al. (2005), the large-signal scattering function can be considered as a linearization that relates the incident and reflected wave coefficients of a weakly nonlinear, time-invariant device (J. Verspecht, M. V. Bossche, and F. Verbeyst, "Characterizing components under large signal excitation: defining sensible 'large signal s-parameters' ?!" in *9th ARFTG Conference Digest,* June 1997, pp. 109-117.; J. Verspecht, D. F. Williams, D. Schreurs, K. A. Remley, and M. D. McKinley, "Linearization of large-signal scattering functions," *IEEE. Transactions on microwave theory and techniques,* vol. 53, pp. 1369—1376, Apr. 2005.). "Weakly nonlinear" means that the output signals are a stable, single-valued, and continuous function of the input signals around the large-signal operating point (J. Verspecht, D. F. Williams, D. Schreurs, K. A. Remley, and M. D. McKinley, "Linearization of large-signal scattering functions," *IEEE. Transactions on microwave theory and techniques,* vol. 53, pp. 1369-1376, Apr. 2005.). It also hints that the spectral components in the output signals are linear combinations with integer coefficients of the frequencies at the input port.

The input and output variables are defined in the frequency domain as depicted in FIG. 2. A_{ij} denotes the complex number representing the j^{th} spectral component of the incident voltage wave at port "i" and B_{ij} denotes in a similar manner the scattered voltage waves. The relationship between the input and output wave signals can be described by Equation 8, with all the spectral components normalized to A_{11} in phase.

$$B_{ij} = S_{ij}(\mathrm{Re}(A_{11}), \mathrm{Re}(A_{12}), \mathrm{Im}(A_{12}), \cdots, \mathrm{Re}(A_{2N}), \mathrm{Im}(A_{2N})) \quad (8)$$

The S_{ij} is called "large-signal scattering function". It is a complex multi-dimensional nonlinear function. If there is only one large tone present at the input and all other harmonic signals are relatively small, it is possible to simplify (or linearize) the multidimensional nonlinear function S_{ij}. Based on this assumption, the superposition principle holds for the harmonics, which can be expressed in Equation 9:

$$B_{ij}(|A_{11}|) = \sum_{q} \sum_{l=1,\cdots,M} S_{iq,jl}(|A_{11}|)P^{j-l}A_{ql} + \sum_{q} \sum_{l=1,\cdots,M} T_{iq,kl}(|A_{11}|)P^{j+l}A^{*}_{ql} \quad (9)$$

$$T_{p1,k1} = 0 \quad (10)$$

where P is the phase of A_{11}. This equation shows that the scattered wave B_{ij}, the j^{th} harmonic at port i, is the sum of incident waves and their conjugates of ilth harmonic at port q incident waves. The introduction of the complex conjugate terms of the incident waves is the consequence of the linearization around the time- varying operating point established by the single large-amplitude tone in the absence of perturbation (J. Verspecht, D. Root, J. Wood, and A. Cognata, "Broad-band, multi-harmonic frequency domain behavioral models from automated large-signal vectorial network measurements," in *IEEE MTT-S Digest,* June 2005.; J. Verspecht, D. F. Williams, D. Schreurs, K. A. Remley, and M. D. McKinley, "Linearization of large-signal scattering functions," *IEEE. Transactions on microwave theory and techniques,* vol. 53, pp. 1369-1376, Apr. 2005.). Equation 10 is required to include the fundamental tones in Equation 9. $S_{iq,jl}$ and $T_{iq,jl}$ are dependent on the magnitude of the A_{11} that models the nonlinear performance of the amplifiers or devices.

Creation of the large-signal scattering function model

The large-signal scattering function of a device can be derived from measurement results using LSNA. A LSNA (sometimes called vector nonlinear network analyzer, or VNNA) is composed of the testset, down-converter, digitizer and analysis software, as shown in FIG. 3. The source 1 is a signal generator that can generate CW signals as well as modulated signals, if required. Source 2 provides the perturbation signal to port 1 or 2 through the switch. This signal simulates the small perturbation signal presented in the model.

The measurement system requires specific multi-tone phase calibration, in addition to the traditional VNA calibration (such as the SOLT or LRM calibration) and absolute

power calibration. The phase calibration normalizes all the fundamental and harmonic spectral components to the phase of A_{11}, the dominant tone at the port 1.

To obtain the coefficients in the large-signal behavioral model for a device, several measurements are required. An example can be used to explain this process. If one is interested in the scattered wave B_{21}, the fundamental tone at port 2. Assume this wave variable is determined by the input large signal tone A_{11} at one specific power level and the spectral components at port 2, including A_{21}, A_{22} and A_{23}. The B_{21} can be written in Equation 11:

$$B_{21} = S_{21,11}A_{11} + S_{22,11}A_{21} + T_{22,11}A_{21}^{*}P^{2} + S_{22,12}A_{22}P^{-1} + T_{22,12}A_{22}^{*}P^{3} + S_{22,13}A_{23}P^{-2} + T_{22,13}A_{23}^{*}P^{4} \quad (11)$$

There are 7 unknown coefficients for this specific power level and frequency. Since superposition holds, as the theory assumes, the 7 coefficients can be obtained through three measurements:

- measurement with only the large-signal A_{11} present;
- two measurements with the small-signal perturbation A_{21} at different phase relative to the A_{11};
- two measurements with the small-signal perturbation A_{22} at different phase relative to the A_{11};
- two measurements with the small-signal perturbation A_{23} at different phase relative to the A_{11};

By combining all these measurement datasets and applying a least-square-error fit, the 7 coefficients can be determined thereafter. By sweeping the amplitude of the A_{11}, a table for the 7 coefficients corresponding to each input signal amplitude can be produced. Then either a look-up-table (LUT) model or an fitting function (e.g. ANN model) can be used to implement the large-signal model in commercial microwave simulation software to simulate the device performance.

If only the fundamental frequency is considered in the large-signal model, that is the harmonic spectral components don't appear in the model, the large-signal model is reduced to so called the "Hot" S22 method (J. Verspecht, "Everything you've always wanted to know about hot-s22 (but we're afraid to ask)," in *Workshop at the International Microwave Symposium,* June 2002.). Equation 12 illustrates this model:

$$B_2 = S_{21}(|A_1|)A_1 + S_{22}(|A_1|)A_2 + T_{22}(|A_1|)P^2A_2^* \quad (12)$$

As pointed out in Verspecht & Esch (1998), the measurements are actually a combination of passive and active (harmonic) loadpull measurements, since the second synthesizer injects signals to the DUTs to simulate the variation in the load (J. Verspecht and P. V. Esch, "Accurately characterizing hard nonlinear behavior of microwave components with the nonlinear network measurement system: Introducing 'nonlinear scattering functions'," in *Proceedings of the 5th International Workshop on Integrated Nonlinear Microwave and Millimeterwave Circuits,* Oct. 1998, PP. 17-26.). Thus, there is the possibility to approximately create the large-signal model from a general loadpull measurement dataset.

Current loadpull-based modeling technique and their limitations

There are several existing techniques to utilize the loadpull dataset for modeling purposes (J. Olah and S. Gupta, "Power amplifier design using measured loadpull data," *Microwave Engineering Europe,* Aug. 2003.; R. L. Carlson, "Meld load-pull test with eda tools," *Microwave and RF,* Apr. 2003.; W. Clausen, J. Capwell, L. Dunleavy, T. Weller, J. Verspecht, J. Liu, and H. Ar- sian, "Black-box modeling of rfic amplifiers for linear and non-linear simulations," *Microwave Product Digest,* Oct. 2004.). Some commercial microwave simulation software packages provide the capabilities to read the loadpull data files into the simulator for linear or nonlinear simulation (Advanced Design System from Agilent Technologies, Inc., CA, USA, www.agilent.com.; Microwave Office from Applied Wave Research, Inc.,CA, USA, www.microwaveoffice.com.).

Generally these techniques can be grouped into two categories: file-based modeling and analytical modeling. As the name suggests, the file-based techniques provide a solution to directly access the loadpull data file through some indexing design to find out the device performance according to a set of rules. Advanced Design System from Agilent Technologies, Inc., Microwave Office from Applied Wave Research, Inc., Olah & Gupta, and Carlson belong to this category (Advanced Design System from Agilent Technologies, Inc., CA, USA, www.agilent.com.; Microwave Office from Applied Wave Research, Inc.,CA, USA, www.microwaveoffice.com.; J. Olah and S. Gupta, "Power amplifier design using measured loadpull data," *Microwave Engineering Europe,* Aug. 2003.; R. L. Carlson, "Meld load-pull test with eda tools," *Microwave and RF,* Apr. 2003.)

Carlson described a method to integrate the loadpull dataset in microwave simulation software for optimization of the load condition for different goals (e.g. output power or IP3) (R. L. Carlson, "Meld load-pull test with eda tools," *Microwave and RF,* Apr. 2003.). Instead of sweeping the amplitude and phase of the reflection coefficient of the load Γ_L, it was proposed to sweep the resistance and capacitance based on the observation of the small-signal S22 seen at the output port of the DUT. This method can capture the frequency effect through the capacitance, which makes the data processing easier. However, this method has its limitation in that it only provides a way to observe the loadpull data file and find the optimal load points for specific goals. It doesn't provide a usable behavioral model for general simulation purposes.

Olah et al. introduced a systematic method to create behavioral models based on the loadpull data file (J. Olah and S. Gupta, "Power amplifier design using measured loadpull data," *Microwave Engineering Europe,* Aug. 2003.). The method has three steps:

- scattered data interpolation: triangulation is used to generate a set of triangular mesh; the contours are plotted by traversing these triangular patches;

- convert the triangulated scattered data to a grid (regular or uniform data) for easy usage in simulators;

• calculate the incident and scattering waves as functions of load impedances using the gridded datasets; the results are stored in a file for access during simulation.

The limitation of this method is that it requires the storage of large data files; much of the information may be redundant. For example, when the input signal level is low, a simple small-signal S-parameter model is enough to predict the gain at various loads. However, this method would utilize the stored B_1 and B_2 for every possible load, which will require a large data file. The extensive file access operation makes this method inefficient.

Another limitation of this method is that the file-based model requires a large number of testing load points to be able to interpolate or extrapolate smoothly on the Smith chart. FIG. 4 illustrates this problem. As can observed, the file-based model doesn't extrapolate the output power contours properly. Analytic models are able to overcome this problem, as will be shown.

Clausen et al. is an example of the use of analytic methods to model the loadpull performance of a device (W. Clausen, J. Capwell, L. Dunleavy, T. Weller, J. Verspecht, J. Liu, and H. Ar- sian, "Black-box modeling of rfic amplifiers for linear and non-linear simulations," *Microwave Product Digest,* Oct. 2004.). By expanding the linear S-parameter through a nonlinear S_{21} function, the model was able to predict the gain compression effects. This is often called "large-S21" method. This technique provides a simple solution to predict the nonlinear performance of the DUT based on the loadpull measurements. However, the large-S21 model has limited accuracy in predicting the gain/phase compression and intermodulation performance at different load conditions.

Due to the limitation of the current modeling techniques based on the loadpull measurement datasets, a new approach is proposed to address the limitations. The new modeling technique exploits the large-signal scattering function theory and derives the relationship between the incident and scattering waves through the loadpull measurement datasets. The detail analysis is given in the following section.

Behavioral model based on loadpull gain and phase compression measurements

A power amplifier can be treated as a two-port network, as shown in FIG. 5. A typical one-tone loadpull measurement gives information about the source impedance (or reflection coefficient, Γ_S) load impedances (or reflection coefficient, Γ_L), the input power (P_{in}), the measured delivered power (P_{out}). For simplicity, suppose the device is unilateral (i.e. $S_{12} = 0$), the input impedance of the port 1 can be expressed as Equation 13. This constrain can be removed if the input port reflected power is captured in the loadpull measurement.

$$\begin{aligned} Z_{in} &= Z_0 \frac{1+\Gamma_{IN}}{1-\Gamma_{IN}} \\ &= Z_0 \frac{1+S_{11}}{1-S_{11}} \end{aligned} \quad (13)$$

Based on the given information, the voltage and current at port 1 can be calculated through the following steps:

$$Z_S = Z_0 \frac{1+\Gamma_S}{1-\Gamma_S} \quad (14$$

$$P_{in} = \frac{E_S^2}{8Re(Z_S)} \quad (15$$

$$E_S = \sqrt{8Re(Z_S)P_{in}} \quad (16$$

$$V_1 = E_S \frac{Z_{in}}{Z_{in}+Z_S} \quad (17$$

$$I_1 = \frac{V_1}{Z_{in}} \quad (18$$

Therefore, the incident and reflected waveforms at port 1 are calculated as:

$$A_1 = \frac{V_1 + I_1 Z_0}{\sqrt{2Re(Z_0)}} = V_1 M_1 \quad (19$$

$$B_1 = \frac{V_1 - I_1 Z_0}{\sqrt{2Re(Z_0)}} = A_1 S_{11} \quad (20$$

$$M_1 = \frac{Z_0 + Z_{in}}{Z_{in}\sqrt{2Re(Z_0)}} \quad (21$$

The incident and reflected waveforms at port 2 are characterized based on the large-signal scattering function theory, as shown in Equation 22 and Equation 23. The phase of the A_{11}, P, is absorbed into the T_{22} coefficient.

$$B_2 = S_{21}A_1 + S_{22}A_2 + T_{22}A_2^* \quad (22)$$

$$A_2 = B_2\Gamma_L \quad (23)$$

Combining Equation 22 and 23 gives:

$$B_2 = S_{21}A_1 + S_{22}B_2\Gamma_L + T_{22}B_2^*\Gamma_L^* \quad (24)$$

Equation 24 is an implicit expression for B_2; it can be further transformed to an explicit function to simplify the model generation. Assume S_{21}, S_{22} and T_{22} are represented as:

$$S_{21} = c_1 + jc_2$$
$$S_{22} = c_3 + jc_4$$
$$T_{22} = c_5 + jc_6$$

where c_i, $i = 1, \ldots, 6$ are unknowns to be determined.

Suppose $B_2 = B_{2r} + jB_{2i}$ and $A_1 = A_{1r} + jA_{1i}$. B_{2r} and B_{2i} are the real and imaginary parts of $B2$ respectively. A_{1i} and A_{1r} are the real and imaginary parts of A_1, respectively. Equation 24 can be rewritten as:

$$(c_1 + jc_2)A_1 + (k_1 + jk_2)B_2 + (m_1 + jm_2)B_2^* = 0 \quad (25)$$

where

$$k_1 + jk_2 = (c_3 + jc_4)\Gamma_L - 1 \quad (26)$$

$$m_1 + jm_2 = (c_5 + jc_6)P^2\Gamma_L^* \quad (27)$$

Arrange the real and imaginary part and we can get:

$$\begin{bmatrix} c_1 A_{1r} - c_2 A_{1i} \\ c_1 A_{1i} + c_2 A_{1r} \end{bmatrix} + \begin{bmatrix} k_1 + m_1 & -k_2 + m_2 \\ k_2 + m_2 & k_1 - m_1 \end{bmatrix} \begin{bmatrix} B_{2r} \\ B_{2i} \end{bmatrix} = 0 \quad (28)$$

By solving the linear function 28, the real and imaginary part of B_2 can be derived as:

$$\begin{bmatrix} B_{2r} \\ B_{2i} \end{bmatrix} = \frac{1}{D} \begin{bmatrix} (k_1 + k_2 - m_1 - m_2)c_1 & (-k_1 + k_2 + m_1 - m_2)c_2 \\ (k_1 - k_2 + m_1 - m_2)c_1 & (k_1 + k_2 + m_1 + m_2)c_2 \end{bmatrix} \begin{bmatrix} A_{1r} \\ A_{1i} \end{bmatrix} \quad (29)$$

where $D = k_1^2 - k_2^2 - m_1^2 + m_2^2$

Obviously, in order to obtain the B_{2r} and B_{2i}, the measurements for both the magnitude and phase are required. This is why it is important to obtain the loadpull AM-PM datasets. The loadpull AM-AM measurements provide the optimization criteria for the magnitude, while the loadpull AM-PM measurements set up the rule for the phase optimization.

The magnitude can be derived from the delivered output power. The output power at port 2 is determined by the A_2 and B_2 through:

$$\begin{aligned} P_{out} &= \frac{1}{2}(|B_2|^2 - |A_2|^2) \\ &= \frac{1}{2}|B_2|^2(1 - |\Gamma_L|^2) \end{aligned} \quad (30)$$

Since the output power is known through the measurement, the $B2$ can be expressed as:

$$|B_2| = \sqrt{\frac{2P_{out}}{1 - |\Gamma_L^2|}} \quad (31)$$

Optimization process can be applied to obtain the 6 unknown coefficients *c1* to *c6*. The least-mean-square (LMS) errors for the magnitude and phase can be represented by Equation 32 and 33.

$$err_{mag} = \frac{\sum_{n}((B_{2r}^2 + B_{2i}^2) - (\frac{1}{1-|\Gamma_L|^2}P_{out}))^2}{n} \quad (32)$$

$$err_{phase} = \frac{\sum_{n}(\Phi(\frac{A2+B2}{A1+B1}) - \text{AM-PM})}{n} \quad (33)$$

where n is the number of load points used in the optimization process. AM-PM is the phase compression data obtained through the loadpull AM-PM measurement. It is the phase difference between the voltages at the input and output ports. The input and output voltages are the sum of the incident and reflected waves at the port respectively.

The analysis given above has been implemented in a Matlab program (The MathWorks, Inc., MA, USA, www.mathworks.com.). FIG. 6 demonstrates the procedure to generate the behavioral model based on the loadpull datasets. Notice that the loadpull datasets can come from either the measurements or from simulations, depending on the applications of this modeling technique.

The invention is described below in examples which are intended to further describe the invention without limitation to its scope.

Example 1: measurement-based behavioral model

To demonstrate the modeling technique proposed in previous section, three example models are created and compared with existing techniques. The three examples are

chosen so that they show two types of applications of this behavioral modeling technique. The first two example models are created based on measurement results, showing an efficient way to integrate measurement results into design. The third example is based on the simulation results, which will lead to decrement in computing complexity and therefore the simulation time.

1.1. Example model of a packaged RFIC LNA

The first example component used is an MAX2373 low noise amplifier (LNA). FIG. 7 shows this component. This component was characterized at 900 MHz. Loadpull gain and phase compression measurements were performed. Two tone load- pull measurements were performed as well. The Matlab modeling program was used to process the measurement data files and generate the model coefficients through the unconstraint nonlinear optimization procedure. In addition, a file-based model is created for characterizing the 3rd order intermodulation products.

The model was implemented in ADS 2004A using the frequency domain defined device (FDD). The advantage of using this device is that it provides the ability to define the behavior of individual frequency components separately. The model only requires two setup parameters: the fundamental frequency (RFfreq), and the frequency spacing (fspacing). For one tone simulation, the fspacing is set at 0. Therefore, the model requires minimum interaction from the users and makes it easy for usage.

The measurement condition is summarized in the following:

- Frequency: 900 MHz;
- Input power: -30 dBm to 5 dBm;
- Two tone frequency spacing: 100 KHz;
- AGC Bias: 1.3875 V;
- Vcc bias: 2.775 V.

FIG. 8 compares the measured and simulated gain and phase compression performance of this LNA at 50 ohm condition. The model predicts the compression property correctly.

FIG. 9 shows the simulated output power contours compared with the measured result. The input power is low at -30dBm. Good agreement is observed. In fact, the large signal model reduces to small-signal S-parameter model when the input signal is low enough. The variation of the output power with respect to the load can be characterized through the small-signal S-parameter. Detailed analysis can be found in Gonzalez (G. Gonzalez, *Microwave Transistor Amplifiers: Analysis and Design (2nd Edition)*. Prentice Hall, 1996.). Compared with the file-based model, obviously the analytic model provides much better interpolation and extrapolation characteristics.

However, the small-signal S-parameter cannot predict accurately nonlinear effects associated with large input signal. The simple large-S21 model provides limited prediction accuracy, compared with the proposed model, as shown in FIG. 10. In this figure, the measured output power contour at input signal of -5dBm is compared with the large-signal model in (a) and the model based on the large-S21 technique in (b). By looking at (a), one can see that the proposed behavioral model does a decent job in predicting the change in the load impedance for optimal output power performance. However, the simple large-S21 modeling technique assumes the compression properties at all load points are the same. This explains why the large-S21 model behaves different from the proposed large-signal model.

Since only the fundamental tone is considered in the model generation, its capability to predict the intermodulation products is limited. Therefore, a file-based model is implemented for prediction of the 3rd order intermodulation products. A contour interpolation algorithm is utilized during the generation of the data file.

FIG. 11 illustrates the comparison of the measured and simulated IP3. The input power is -20dBm. As can be seen, the behavioral model does a good job predicting the IP3 performance over a defined region.

Six load impedances are chosen as examples to test the large-signal model. The simulated fundamental tone and the 3rd order intermodulation product are compared

with the measurement results. The reflection coefficients of the 6 example loads are listed in Table 1 and plotted in Smith Chart, as shown in FIG. 12. The load examples are chosen to spread over the Smith Chart.

(a)	0.56723+j*0.03630	(b)	0.36904+j*0.40569
(c)	0.75532+j*0.50893	(d)	0.77211+j*0.16110
(e)	0.17539+j*0.76875	(f)	0.30559-j*0.57057

Table 1. List of the six example load reflection coefficients used to test the LNA model.

The simulated results are compared with corresponding measurement datasets in FIG. 13. Good agreements can be observed for all cases. Also given out are the simulated results obtained from the large-S21 model. The large-S21 model presents good performance for limited set of load points, such as at (a), (d), (e), and (f). However, at (b) and (c) the simulation results show significant discrepancies. Therefore, the new large-signal behavioral model provides better performance against the large-S21 behavioral model.

FIG. 14 shows the errors in the simulated fundamental tone at different loads. As can be seen, the new model has much less errors compared with the large-S21 model. Similarly, FIG. 15 illustrates the errors in the simulated IM3 at different loads. Again, the new model has better performance compared with the large-S21 model.

1.2. Example model of a PA sample

The second example component used is an Intersil power amplifier (ISL3984). FIG. 16 shows the tested ISL3984 power amplifier sample. Loadpull gain and phase compression measurements were performed on this power amplifier sample at 2450 MHz. The measurement condition is summarized below:

- Frequency: 2450 MHz;
- Input power: -20 dBm to 0 dBm;

- Two tone frequency spacing: 100 KHz;
- Bias: 3.3 V.

To verify the performance of the behavioral model, a swept power harmonic simulation is done in 50 ohm condition, i.e. the source and load impedances are at 50 ohm. The simulated gain and phase compression curves are compared to the measured data in FIG. 17. Good agreement can be seen in the figure.

FIG. 18 compares the simulated and measured output power contours at input power level of -20dBm. The source impedance is set to be conjugately matched. The Γ_s is 0.34051 + j * 0.58271. As can be seen, the two datasets agree very well.

Similar to the LNA model, a file-based model is created for the simulation of IM3. FIG. 19 compares the simulated and measured IM3 contours at input power level of -20dBm. The file-based model predicts the 3rd order intermodulation product accurately under various load conditions.

Six load impedances are chosen as examples to test the large-signal model. The simulated fundamental tone and the 3rd order intermodulation product are compared with the measurement results. The reflection coefficients of the 6 example loads are listed in Table 4.2 and plotted in Smith Chart, as shown in FIG. 20. The load examples are chosen to spread over the Smith Chart.

(a)	0.62561+j*0.39360	(b)	-0.36966+j*0.09652
(c)	0.19215+j*0.33529	(d)	0.87741+j*0.07210
(e)	0.61180+j*0.627895	(f)	0.52078-j*0.53337

Table 2. List of the six example load reflection coefficients used to test the PA model.

The simulated results are compared with corresponding measurement datasets in FIG. 21. Good agreements can be observed between the simulated results from the proposed model and the measurements. Also given out are the simulated results obtained from the large-S21 model. The large-S21 model presents good performance for limited set of load points, such as at (a), (b), (d), and (e). However, at (c) and (f) the simulation results show significant discrepancies.

Therefore, the new large- signal behavioral model provides better performance against the large-S21 behavioral model.

FIG. 22 shows the errors in the simulated fundamental tone at different loads. As can be seen, the new model has much less errors compared with the large-S21 model. Similarly, FIG. 23 illustrates the errors in the simulated IM3 at different loads. Again, the new model has better performance compared with the large-S21 model.

Through the comparison results illustrated from the two example models, the validity of the model has been proved. The behavioral model derived from the loadpull gain and phase compression measurements can predict the performance of the DUT under various load conditions and input power levels accurately to some extent.

This measurement-based behavioral modeling technique is also demonstrated as simple solution to integrate the loadpull measurement datasets with commercial CAE softwares. The resulted model provides the invaluable insights for designers to study nonlinear components at system levels without losing much accuracy.

Example 2: simulation-based behavioral model

We have discussed the measurement-based behavioral modeling approach in previous section. The second behavioral modeling example will demonstrate the process to derive a abstract model based on the simulation datasets. An equivalent circuit model for the 30 Watts Cree UGF21O3O LDMOS power transistor is used to create the simulation datasets.

This model was simulated at 2.17 GHz under swept power and various load conditions. The simulated AM-AM and AM-PM datasets were used to create the large- signal behavioral model. The simulation setup for generating the test datasets is given below:

- Frequency: 2170 MHz;
- Input power: 0 dBm to 35 dBm;
- Two tone frequency spacing: 100 KHz;

• Bias: Vgs is 4 V and Vds is 25 V (biased for deep Class AB amplifier).

FIG. 24 compares the simulated results from the behavioral model and the circuit model for the gain and phase compression. Good agreements are achieved for the 50 ohm case.

FIG. 25 and FIG. 26 show the delivered power simulated under loadpull conditions, at two input power levels (10 dBm and 30 dBm). The source reflect coefficient is set at -0.55244-j * 0.23757. For the small input power level (10 dBm), the behavioral model presents almost identical performance as the circuit model. Even at high power levels (e.g. 30 dBm), the behavioral model still does a good job to predict the drift in the optimal load impedance for the output power.

As one example to demonstrate the importance to have the loadpull AM-PM information in the model creation, two behavioral models were created, one optimized with the AM-PM information and one without.

FIG. 27 compares the IM3 contours simulated by the behavioral models with and without the AM-PM information. The results are obtained through Envelope simulation of the behavioral model. Obviously, the loadpull AM-PM information does help the large-signal model to do a better job to predict the intermodulation performance. This comparison proves the importance of having the loadpull information for creating a large-signal behavioral model based on loadpull measurements. Notice that not like the previous two example models, the IM3 prediction here doesn't depend on file-based models.

FIG. 28 compares the simulated IM3 contours from the behavioral model (with the AM-PM information) and the circuit model. In general, the model predicts the trend of the IM3 performance. However, since only the fundamental tone is utilized in the model generation, its ability to predict the IM3 is limited. To get better results for the intermodulation products, either file-based model can be used or additional loadpull harmonic measurements will help.

FIG. 29 evaluates the performance of the behavioral model under two tone stimuli against that of the circuit model. The input power is set to sweep in the

simulation. Again, both behavioral models are evaluated. High level agreements can be observed for the simulated datasets from both models.

Notice the difference between the two behavioral models. The model without the AM-PM information predicts a false sweet spot in the IM3 curve. This is avoided through including the AM-PM information in the model generation process.

One advantage using behavioral models instead of circuit models is that behavioral models require less simulation time. This will become important when simulating a complete design system, which usually contains dozens of transistors or more.

Table 3 compares the simulation time using the behavioral model and the circuit model. The loadpull harmonic balance simulation for 100 load points is performed at three different input power levels: 10 dBm, 20 dBm and 30 dBm. This test was performed on a workstation with a Pentium-4 CPU and 1 GB memory. The behavioral model requires less simulation time, especially at high power levels, as can be observed from the table.

Type	10 dBm	20 dBm	30 dBm
BEH. Model	2.55 sec	2.66 sec	2.89 sec
CIR. Model	3.08 sec	3.95 sec	4.05 sec

Table 3. Simulation time comparison: behavioral model vs. circuit model. Loadpull harmonic balance simulation at three input power levels is performed for the test.

Conclusion

A behavioral modeling technique has been presented that is based directly on the loadpull gain and phase compression measurements. Developed from the large-signal scattering function theory, this technique shows the possibility to generate the large-signal scattering function model using traditional loadpull measurement systems. The large-signal scattering function theory is presented and the analogy between the LSNA and the loadpull measurement systems is drawn. A detailed analysis of the model generation process is given out. Three example behavioral

models are created to demonstrate the capability of this new technique. Two of them are based on measurements, while one is based on the simulation dataset from an equivalent circuit model. These models are studied from different aspects, including the one tone loadpull and power swept simulation, two tone loadpull and power swept simulation. Good agreements are observed between the model simulated results and measurements, showing the strong capability of this modeling technique.

The disclosure of all publications cited above are expressly incorporated herein by reference, each in its entirety, to the same extent as if each were incorporated by reference individually.

It will be seen that the advantages set forth above, and those made apparent from the foregoing description, are efficiently attained and since certain changes may be made in the above construction without departing from the scope of the invention, it is intended that all matters contained in the foregoing description or shown in the accompanying drawings shall be interpreted as illustrative and not in a limiting sense.

It is also to be understood that the following claims are intended to cover all of the generic and specific features of the invention herein described, and all statements of the scope of the invention which, as a matter of language, might be said to fall therebetween. Now that the invention has been described,

What is claimed is:

1. A method for characterizing a device under test (DUT) comprising the steps of:

providing a first signal having a first frequency to a first signal port of the DUT as a power tone signal

providing a second signal having a second frequency to a second signal port of the DUT as a probe tone signal,

generating a model from the loadpull dataset.

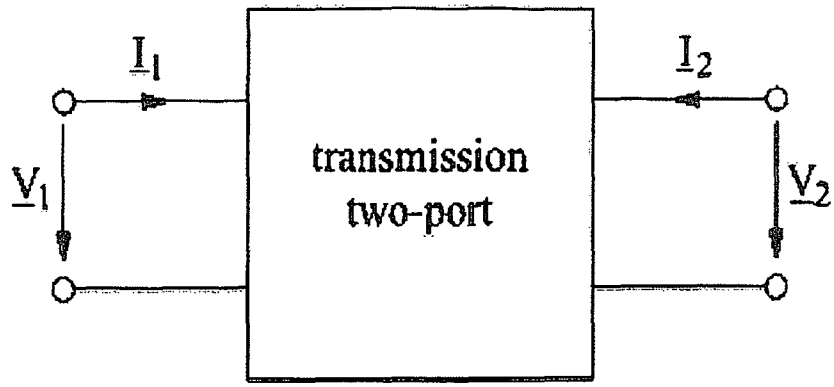
I_1
I_2
V_1
V_2
transmission
two-port

FIG. 1

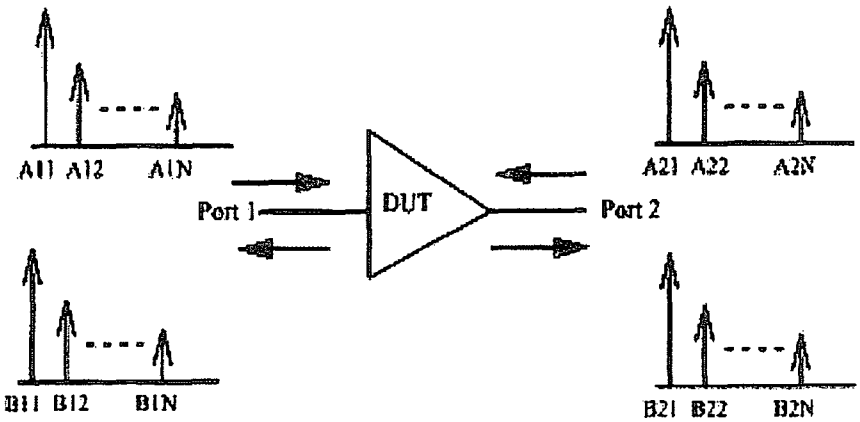
A11 A12 A1N
A21 A22 A2N
Port 1
DUT
Port 2
B11 B12 B1N
B21 B22 B2N

FIG. 2

FIG. 3

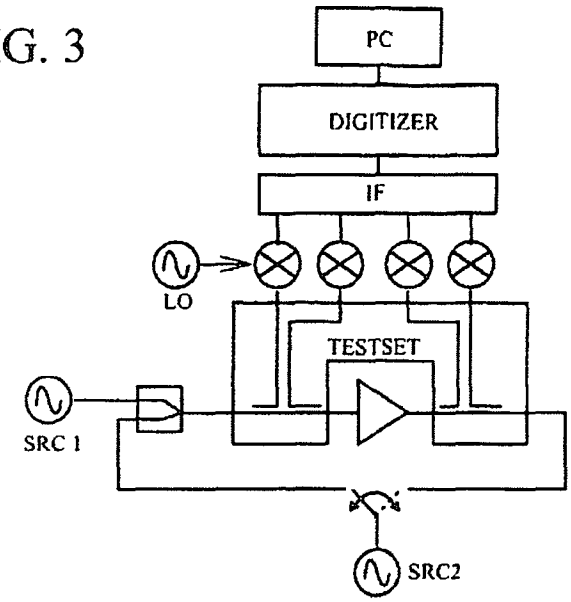
PC
DIGITIZER
IF
LO
TESTSET
SRC 1
SRC2

FIG. 4

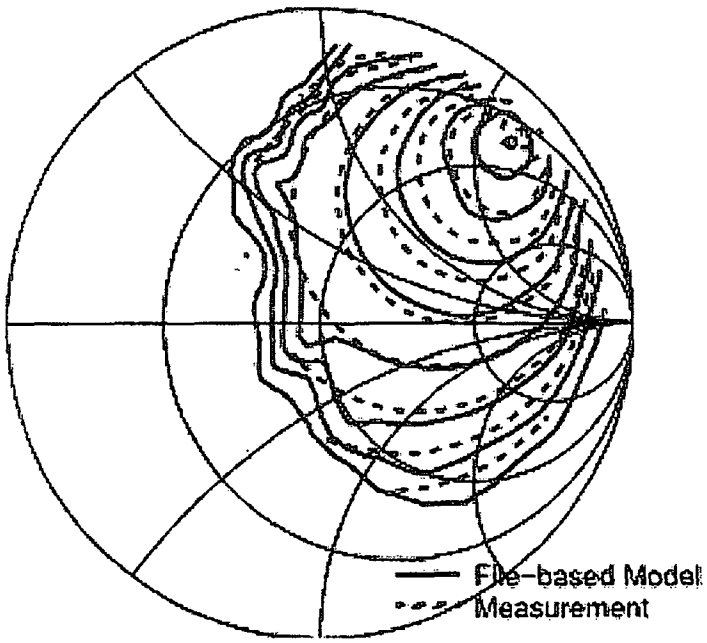
Pout comparison (Pin at -30 dBm): file-based model vs. measurement
File-based Model
Measurement

FIG. 5

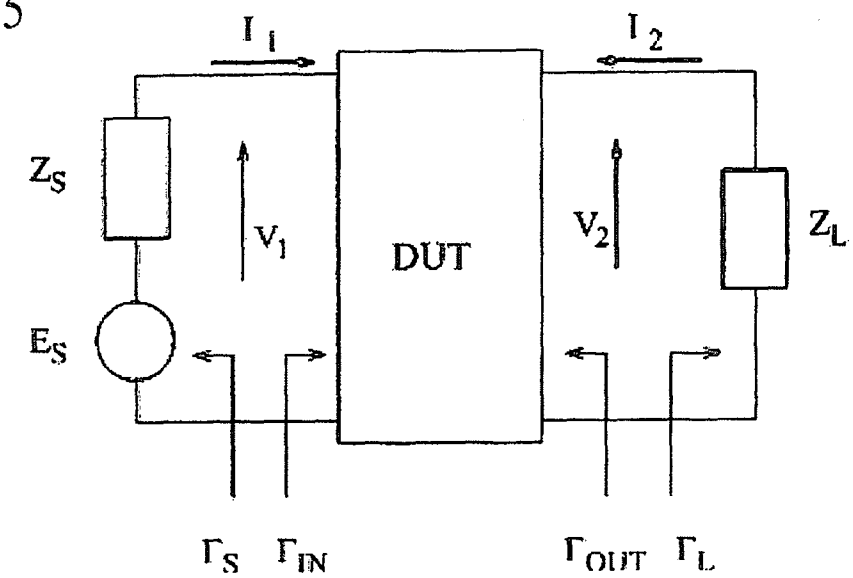
I 1
I 2
Z S
V 1
DUT
V 2
Z L
E S
Γ S
Γ IN
Γ OUT
Γ L

FIG. 6

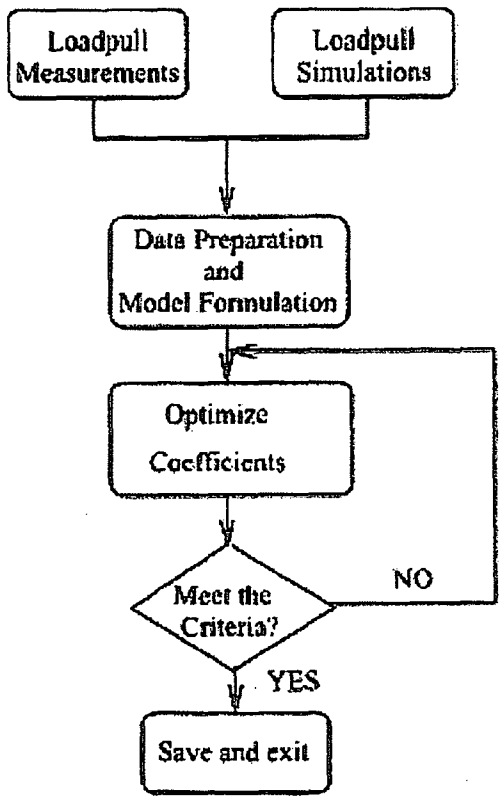
Loadpull Measurements
Loadpull Simulations
Data Preparation and Model Formulation
Optimize Coefficients
Meet the Criteria?
NO
YES
Save and exit

FIG. 7

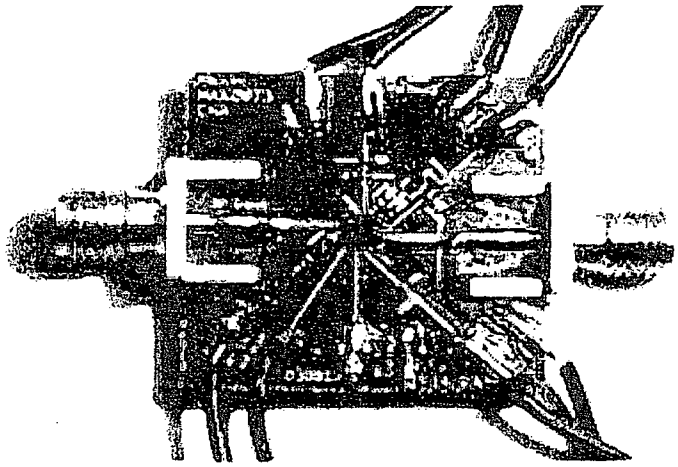

FIG. 8

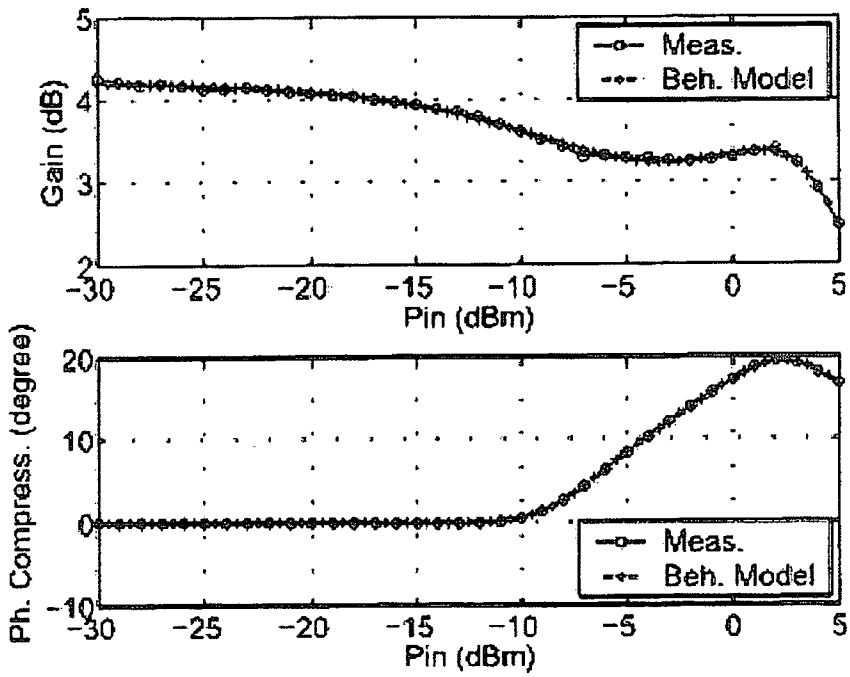
Gain (dB)
Pin (dBm)
Meas.
Beh. Model
Ph. Compress. (degree)
Pin (dBm)
Meas.
Beh. Model

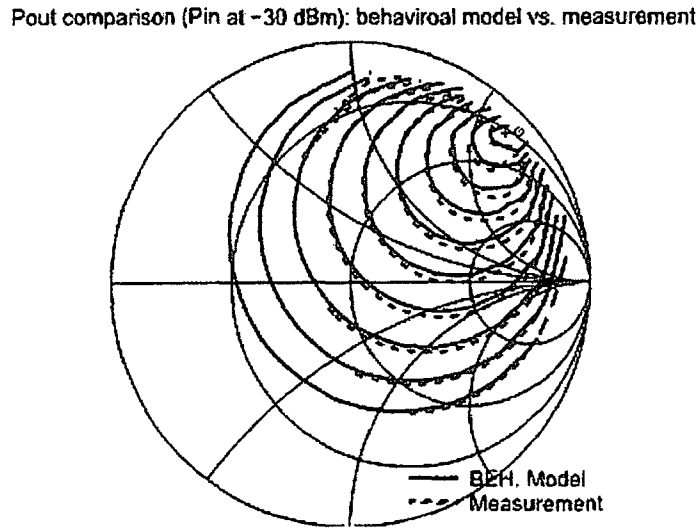
Pout comparison (Pin at -30 dBm): behaviroal model vs. measurement
BEH. Model
Measurement

FIG. 9

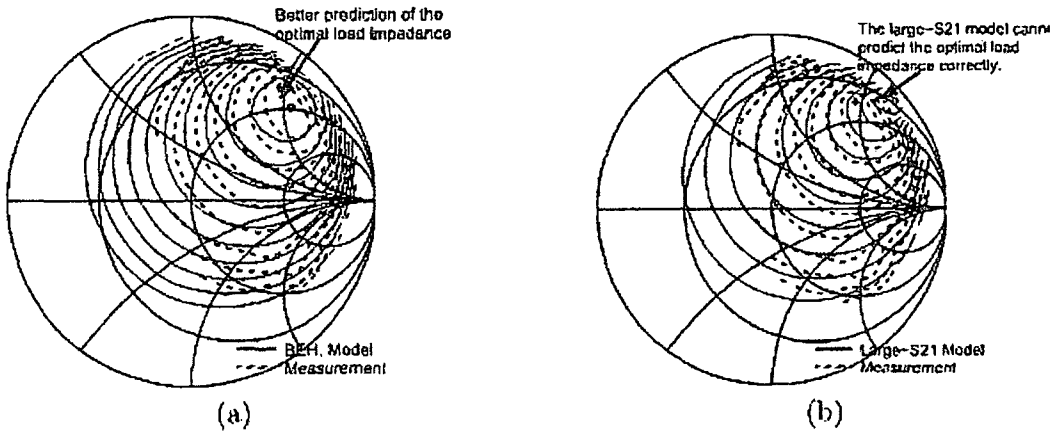
Better prediction of the optimal load impedance
BEH. Model
Measurement
(a)
The large-S21 model can predict the optimal load impedance correctly.
Large-S21 Model
Measurement
(b)

FIG. 10

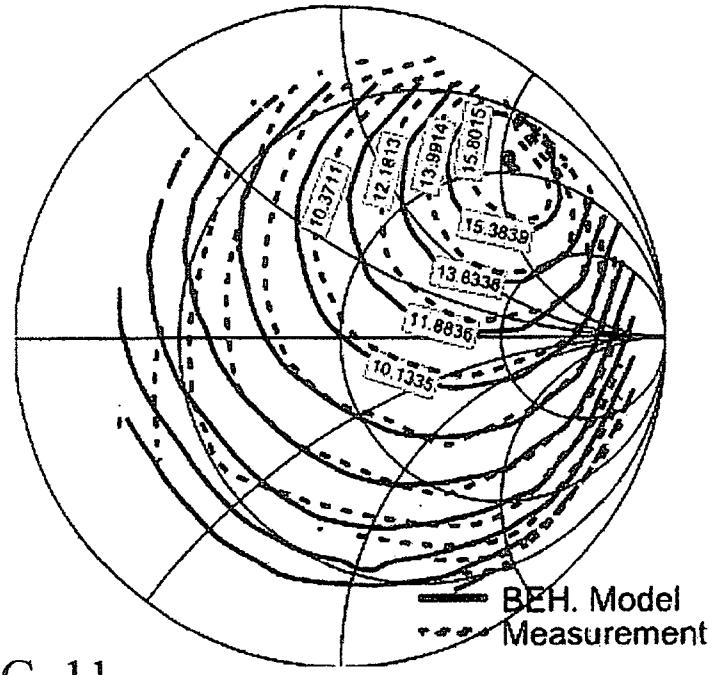
10.3711
12.1813
13.9914
15.8015
15.3839
13.6338
11.8836
10.1335
BEH. Model
Measurement

FIG. 11

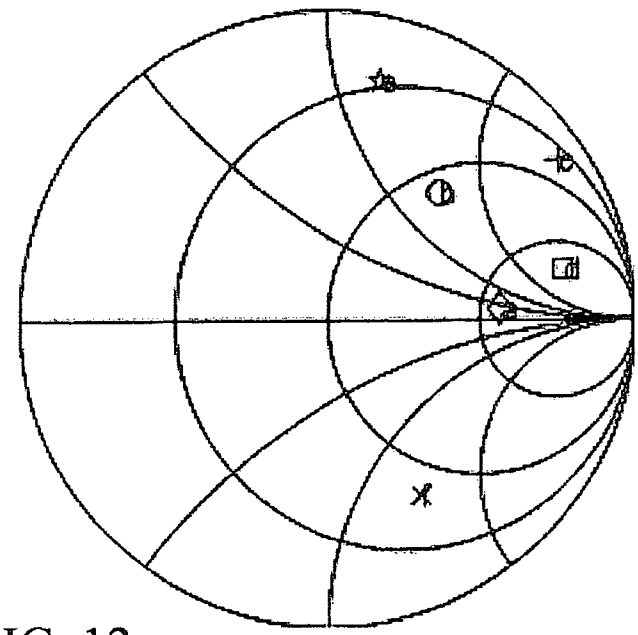

FIG. 12

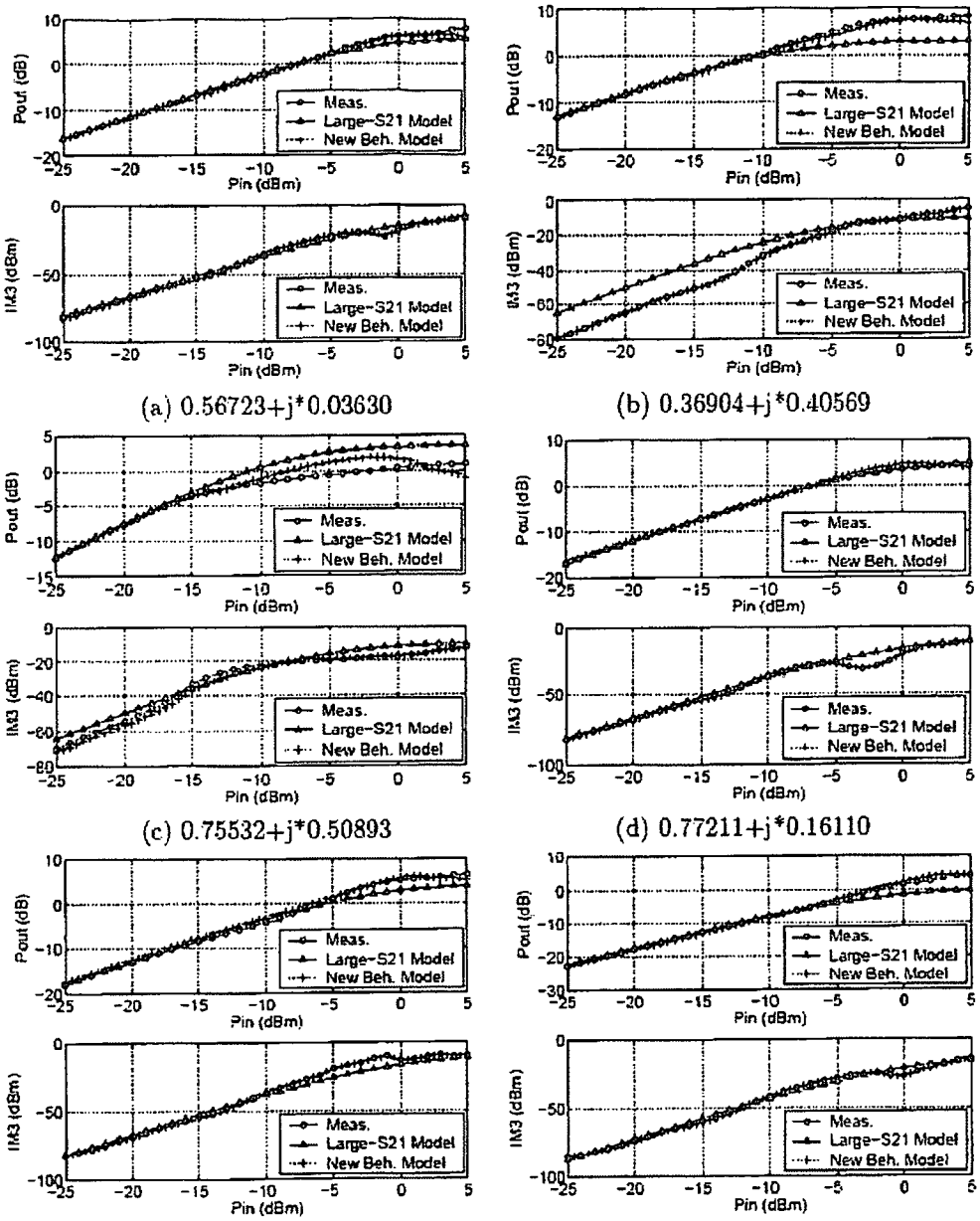

(a) 0.56723+j*0.03630

(b) 0.36904+j*0.40569

(c) 0.75532+j*0.50893

(d) 0.77211+j*0.16110

(e) 0.17539+j*0.76875

(f) 0.30559-j*0.57057

FIG. 13

FIG. 14

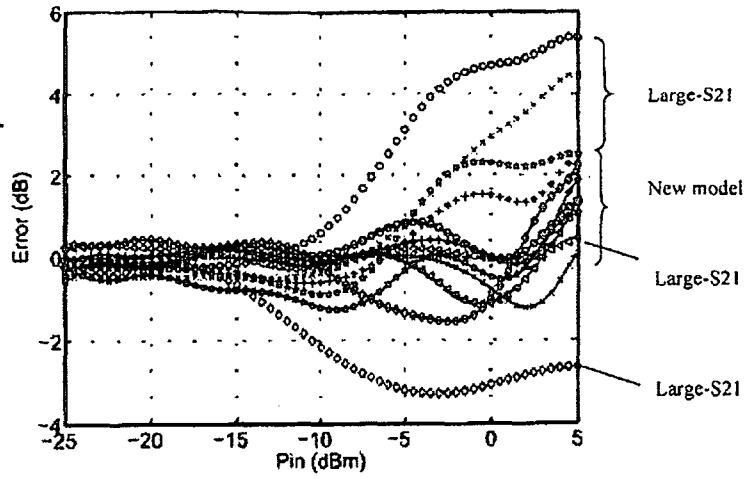
Error (dB)
Pin (dBm)
Large-S21
New model
Large-S21
Large-S21

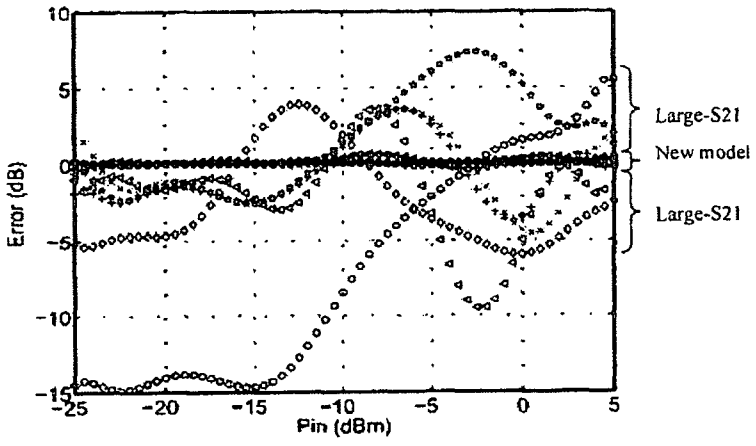
Error (dB)
Pin (dBm)
Large-S21
New model
Large-S21

FIG. 16

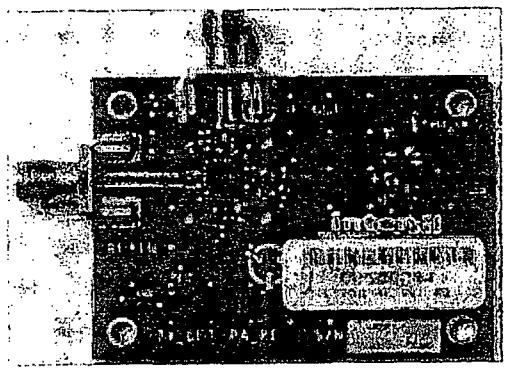

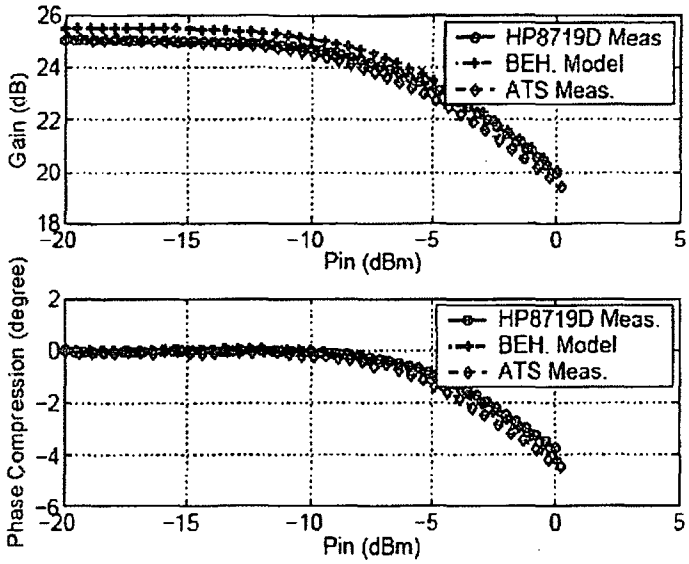
Gain (dB)
Pin (dBm)
HP8719D Meas
BEH. Model
ATS Meas.
Phase Compression (degree)
Pin (dBm)
HP8719D Meas.
BEH. Model
ATS Meas.

FIG. 17

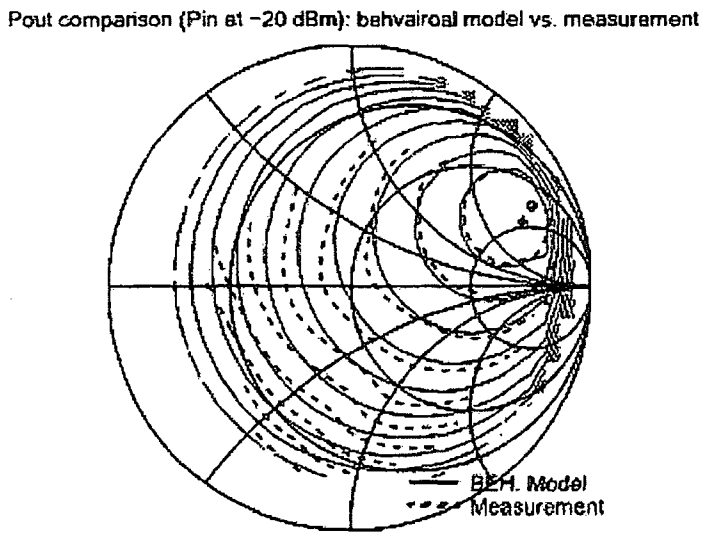
Pout comparison (Pin at −20 dBm): behvairoal model vs. measurement
BEH. Model
Measurement

FIG. 18

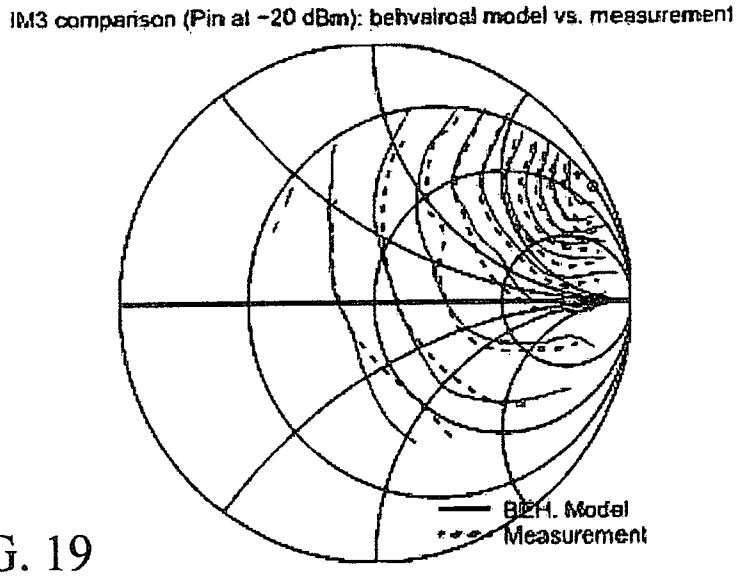
IM3 comparison (Pin at −20 dBm): behvairoal model vs. measurement
BEH. Model
Measurement

FIG. 19

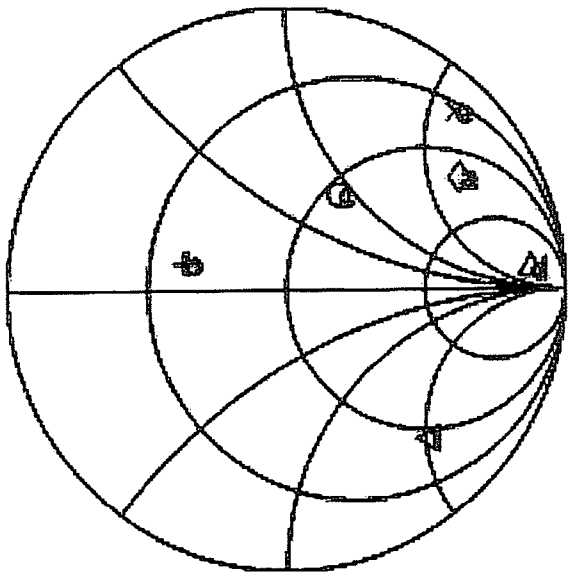

FIG. 20

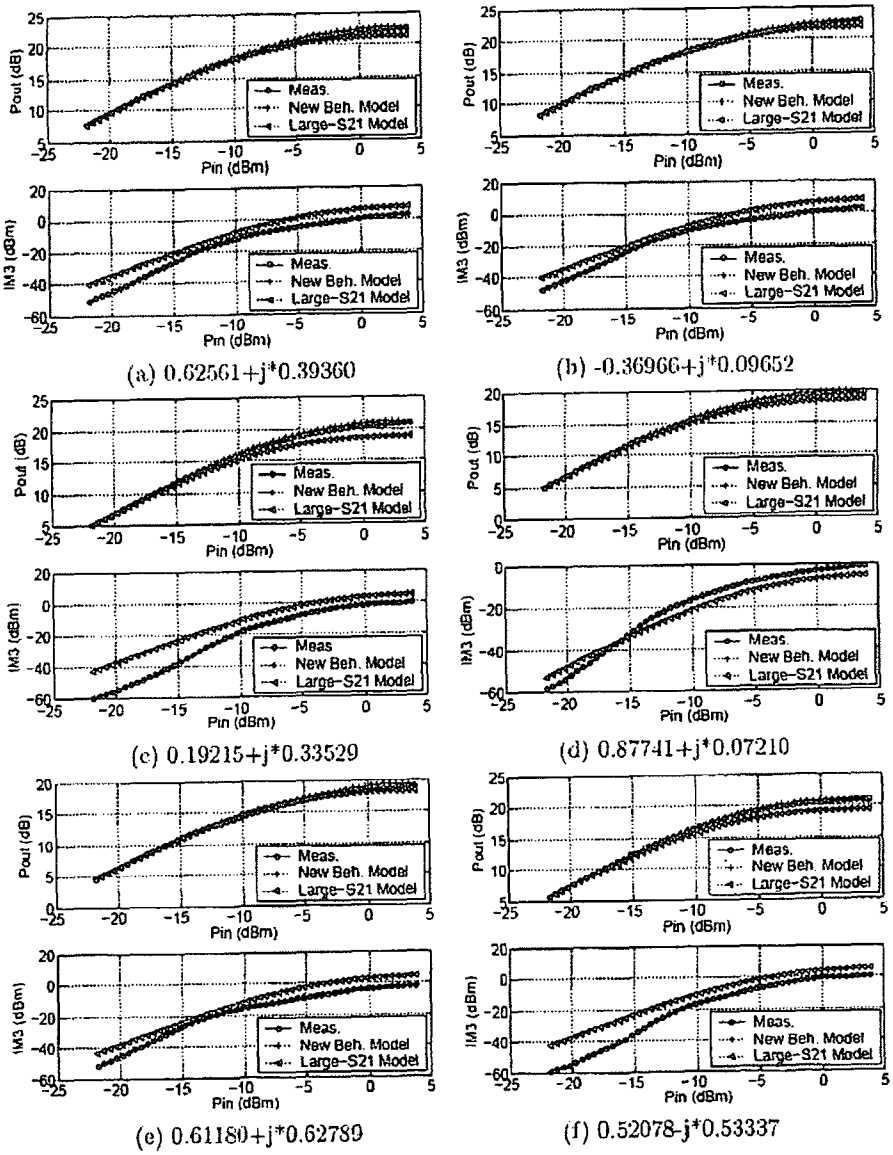

(a) 0.62561+j*0.39360

(b) -0.36966+j*0.09652

(c) 0.19215+j*0.33529

(d) 0.87741+j*0.07210

(e) 0.61180+j*0.62789

(f) 0.52078-j*0.53337

FIG. 21

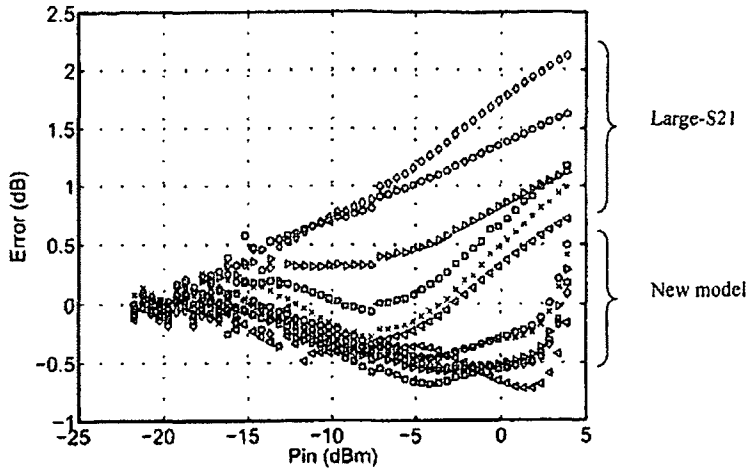
Error (dB)
Pin (dBm)
Large-S21
New model

FIG. 22

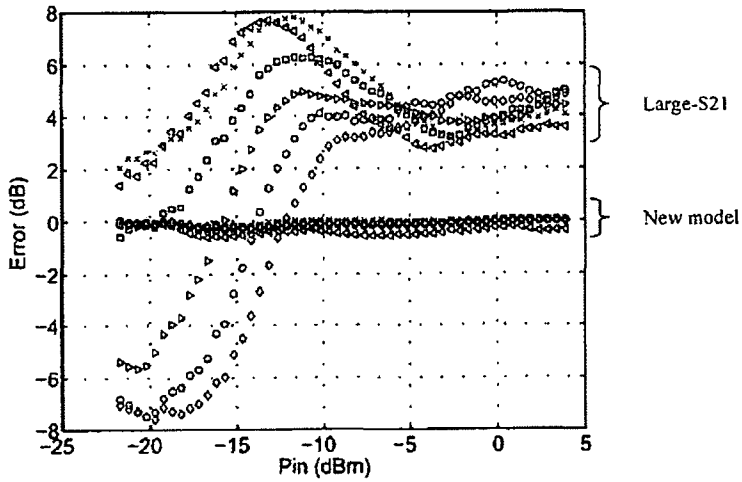
Error (dB)
Pin (dBm)
Large-S21
New model

FIG. 23

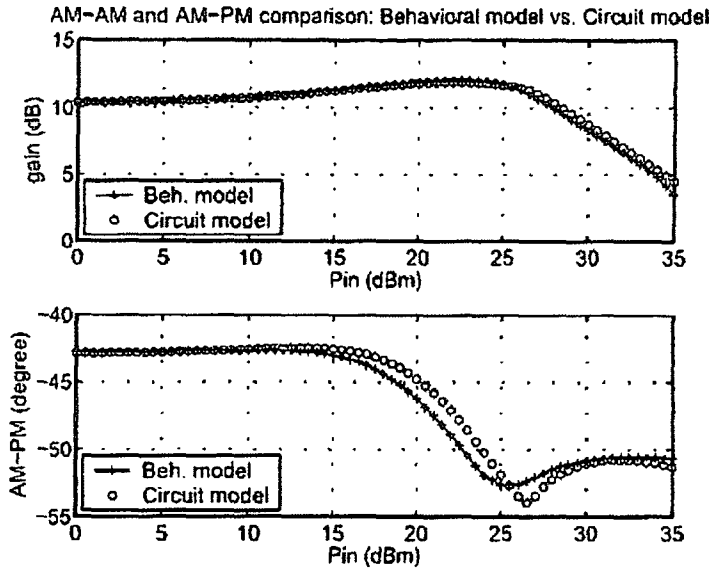
AM-AM and AM-PM comparison: Behavioral model vs. Circuit model
gain (dB)
Beh. model
Circuit model
Pin (dBm)
AM-PM (degree)
Beh. model
Circuit model
Pin (dBm)

FIG. 24

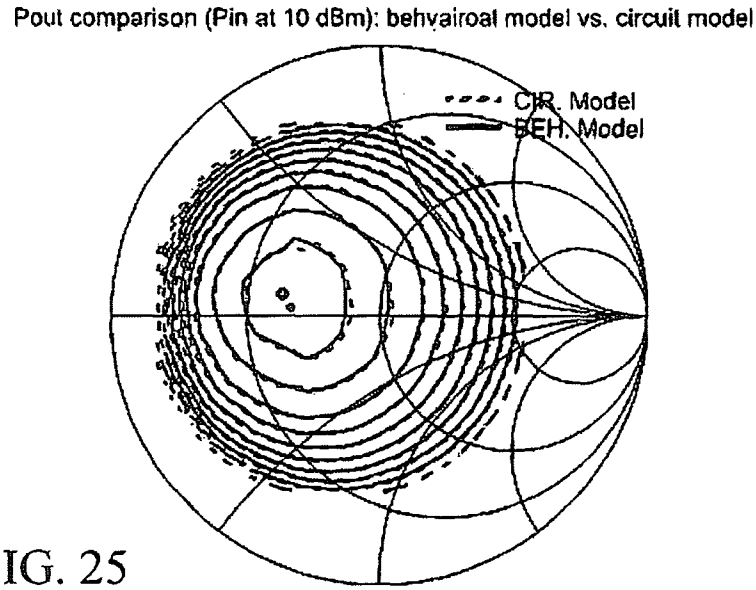
Pout comparison (Pin at 10 dBm): behvairoal model vs. circuit model
CIR. Model
BEH. Model

FIG. 25

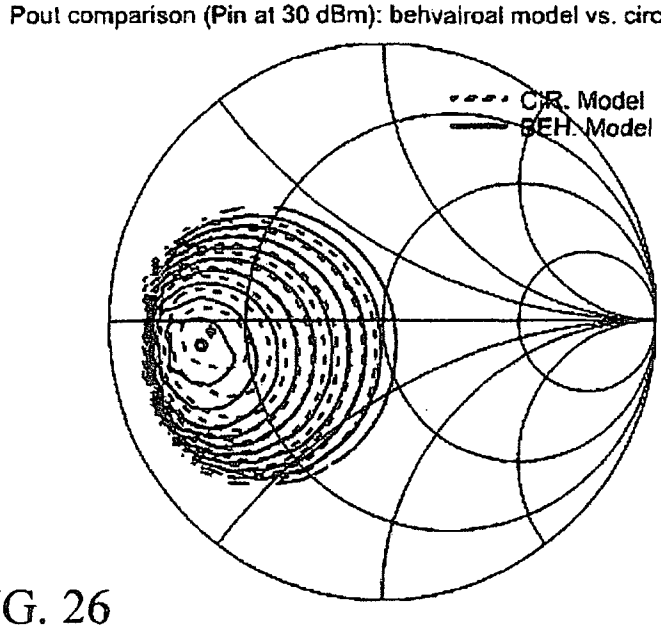
Pout comparison (Pin at 30 dBm): behvalroal model vs. circuit model
C/R. Model
BEH. Model

FIG. 26

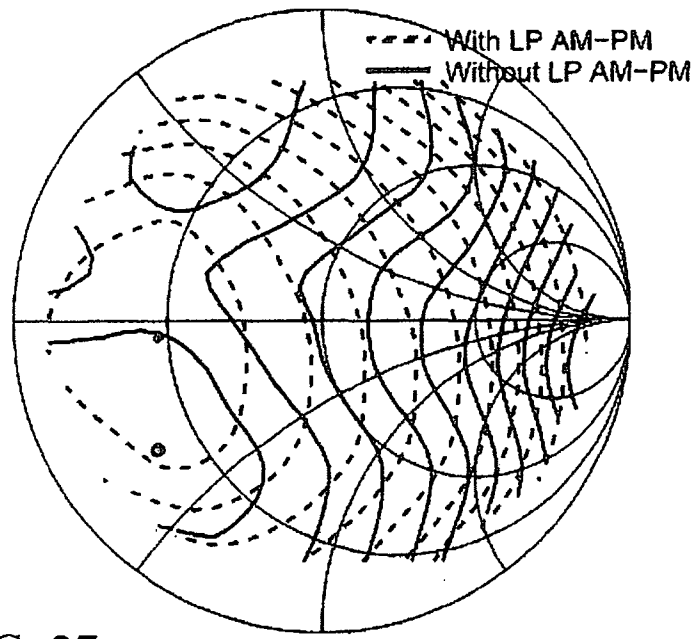
IM3 Comparison for two different behavioral models
With LP AM-PM
Without LP AM-PM

FIG. 27

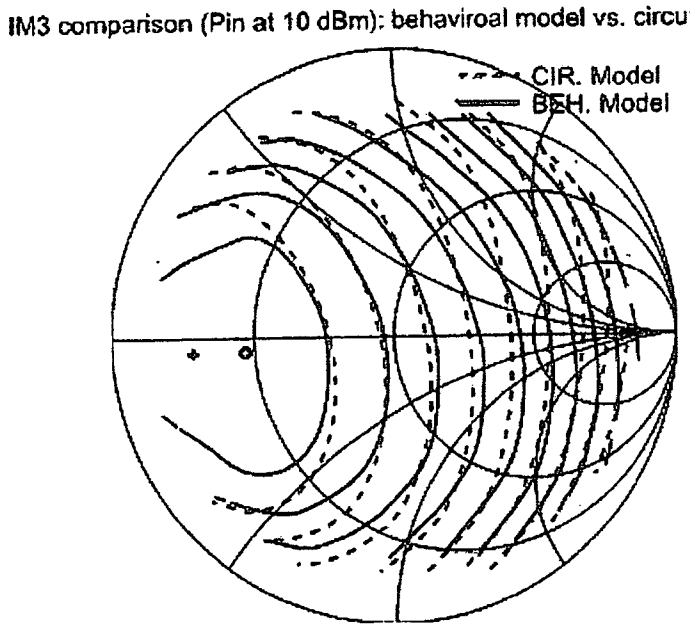
IM3 comparison (Pin at 10 dBm): behaviroal model vs. circuit model
CIR. Model
BEH. Model

FIG. 28

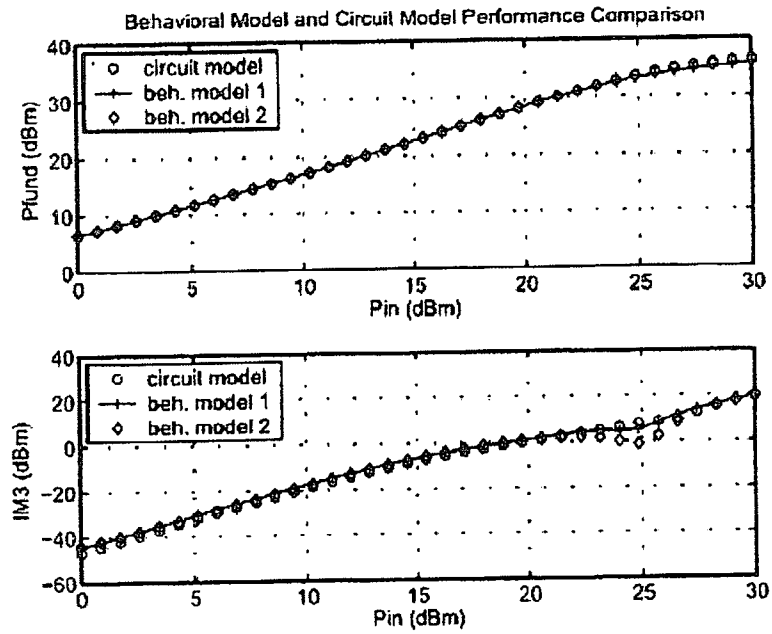
Behavioral Model and Circuit Model Performance Comparison
circuit model
beh. model 1
beh. model 2
Pfund (dBm)
Pin (dBm)
IM3 (dBm)

FIG. 29